

# Fluid–structure interaction during the impact of a cylindrical shell on a thin layer of water

T.I. Khabakhpasheva\*

*Laurentyev Institute of Hydrodynamics, Laurentyev pr.15, Novosibirsk 630090, Russia*

Received 14 December 2007; accepted 11 October 2008

Available online 17 December 2008

---

## Abstract

A two-dimensional unsteady analysis of an elastic circular cylindrical shell that enters a thin layer of an ideal incompressible liquid is considered. The cylinder initially touches the liquid free surface at a single point and then penetrates the liquid layer at a constant vertical velocity. The problem is coupled because the liquid flow, the shape of the elastic shell and the geometry of the contact region between the body and the liquid must be determined simultaneously. The flow region is subdivided into four complementary regions that exhibit different properties: the region beneath the entering body surface, the jet root, the spray jet, and the outer region. A complete solution is obtained by matching the solutions within these four subdomains. The structural analysis is based on the normal-mode method. Strain-time histories of the inner surface of the cylinder are of particular interest. In the case of a very flexible shell three distinct regimes of the impact process were found. For a high impact velocity the lower part of the shell flattens and the shell does not enter the water. For a moderate impact velocity the shell reaches the bottom and an effect of “fluid capture” may occur. For a low impact velocity the shell penetrates the liquid, but the size of the contact region decreases before the shell reaches the bottom. This behaviour corresponds to exit or “reflection” of the shell from the water layer.

© 2008 Elsevier Ltd. All rights reserved.

*Keywords:* Water impact; Fluid–structure interaction; Elastic shell; Thin layer of water; Normal mode method

---

## 1. Introduction

Impact of an elastic cylindrical shell onto water surface became an important practical problem in the 1930s, when hydroplanes were first built. As a hydroplane touches a water surface, its body (approximately a cylindrical shell) or skis (also approximately cylindrical shells) are subject to very high hydrodynamic loads, which need to be properly understood. Fluid–structure interactions are also of considerable practical importance for other engineering fields, e.g., bottom slamming on a bulbous ship bow.

Pioneering works on the slamming problem were done by Von Kármán (1929) and Wagner (1932). Both of these pioneering studies assume (infinitely) deep water and small deadrise angles, which means that the impacting body surface is nearly tangential to the water surface. This assumption allowed Wagner to use the so-called “flat disk approximation”, in which both the dynamic and kinematic free-surface boundary conditions are applied on the

---

\*Tel.: +7 383 333 30 66; fax: +7 383 333 16 12.

*E-mail addresses:* [tana@hydro.nsc.ru](mailto:tana@hydro.nsc.ru), [tkhab@ngs.ru](mailto:tkhab@ngs.ru) (T.I. Khabakhpasheva).

undisturbed free surface. Wagner introduced conditions (nowadays called “Wagner conditions”) at the intersection points between a body and the liquid free surface, which require that the free-surface elevation is equal to the body position at this point. In the Wagner theory the flow velocity is square root singular at the intersection points. Wagner’s approach was adopted in numerous studies of water impact on both rigid and elastic bodies and continue to be actual until now, see e.g., Khabakhpasheva and Korobkin (1997) or Korobkin et al. (2006). A review of these studies may be found in, e.g., Faltinsen et al. (2004) and in Korobkin and Khabakhpasheva (2006).

Another approach was developed by Korobkin (1995) for the case when the body penetration depth is comparable to thickness of the liquid layer. This study considered the impact of two rigid bodies, one of which is covered by a thin liquid layer. These flows are characterized by jets of thickness comparable to the liquid depth but with their roots along the perimeter of the contact region. Korobkin decomposed the liquid layer into four distinct regions and used a matched asymptotic analysis. Korobkin’s method is developed further here for a flexible elastic shell.

Howison et al. (2002) developed a theory of slamming for finite water depth. In this theory, Wagner’s approach and Korobkin’s approach represent limiting cases which correspond to (infinitely) deep water and shallow water, respectively.

Numerical investigations of water entry and exit of a circular cylinder have been reported by many authors. Greenhow (1988) used a boundary element method based on Cauchy’s theorem, and Zhu et al. (2005) used a CIP method. These studies assume rigid bodies. Arai and Miyauchi (1998) and Sun and Faltinsen (2006) investigated two-dimensional hydroelastic fluid–structure interactions during water entry of a cylindrical shell, using a CFD method for the flow field and a modal analysis for the shell structure. Sun and Faltinsen’s (2006) coupled fluid–structure analysis considers finite water depth and includes a comparison of both Wagner’s and Karman’s approaches with the CFD results. Ionina and Korobkin (1999) used the modal analysis to study cylindrical shell impact onto deep water with Wagner’s approach for the liquid flow.

Impact of an elastic shell on a thin liquid layer is considered in this study. The modal approach is used for the structural analysis, and Korobkin’s approach is adopted for the hydrodynamic analysis. Accordingly, the flow region is decomposed into four complementary subdomains, within each of which a distinct flow analysis is performed. A uniformly valid asymptotic solution of the fluid–structure interaction problem is then obtained via matching of the solutions within the four complementary flow regions. The elastic deformation of the shell are taken into account via coupling of a structural analysis and a hydrodynamic analysis.

The coupled problem is formulated in Section 2. General assumptions, decomposition of the flow region and scaling of the liquid flow problem are also considered in this section. The mathematical statement of the structural problem is given in Section 3. The hydrodynamic analysis and matching of the solutions in the complementary subregions are considered in Sections 4 and 5. The coupled hydroelasticity problem is analysed using the normal mode method in Section 6. Numerical results are reported and discussed in Section 7. Finally, concluding remarks are given in Section 8.

## 2. Problem formulation and general assumptions

A two-dimensional analysis of the impact of an elastic circular shell, of radius  $R'$ , on a thin layer  $-h' < y' < 0$  of water, initially at rest, is considered here; see Fig. 1. At time  $t' = 0$ , the cylinder touches the free surface  $y' = 0$  at a point, chosen as the origin of a Cartesian system of coordinates  $x'Oy'$ , and hits the liquid layer with vertical velocity  $V$ . The velocity and shape of the cylinder for  $t' > 0$  vary due to interactions between the elastic cylinder and the liquid. The location of the contact points between the free surface and the elastic body are not known beforehand, and must be determined together with the liquid flow and the shell deformation.

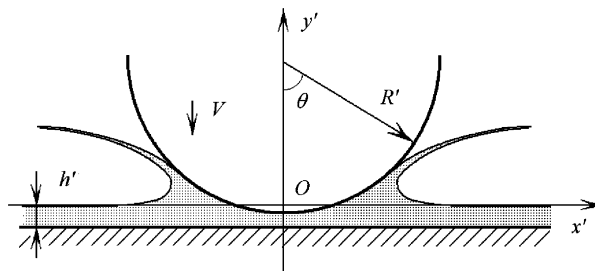


Fig. 1. Definition sketch for the impact of a shell on a thin layer of water.

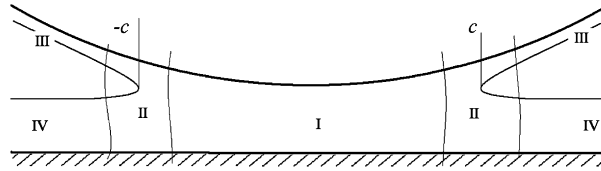


Fig. 2. Definition sketch for the decomposition of the flow region.

The deformations of the elastic cylinder, the distribution of bending stresses, and the location of the contact points are determined under the following assumptions:

- (i) the liquid is ideal and incompressible;
- (ii) the flow in the liquid layer is two-dimensional and symmetrical with respect to the  $y'$ -axis;
- (iii) the liquid flow in the region beneath the entering body is represented using the shallow water model;
- (iv) the shell thickness is constant and small;
- (v) external mass forces and surface tension have negligible effects;
- (vi) the wetted area of the cylinder is a monotonically increasing function of time  $t'$ .

The problem is formulated in nondimensional form, using  $L = h'$  and  $T = h'/V$  as length and time scales,  $V$  as velocity scale for the liquid flow, and  $\rho V^2$  as the hydrodynamic pressure scale; here,  $\rho$  is the liquid density.

The flow is analysed using the method of matched asymptotic expansions; see Korobkin (1995). Specifically, the flow field is divided into four regions, as depicted in Fig. 2. Region I is the region beneath the entering body; region II is the jet root; region III is the spray jet; and region IV is the outer region.

It is important to note that the dimension of region I is not fixed during the impact process, but depends on the size of a contact region. To connect the liquid flow in the four regions, we use conservation laws in region II. The inner geometry of region II is chosen for the case when the dimension of a contact region grows and a jet arises.

The velocity of the fluid particles in the jet root (region II) is tangential to the body surface. In a jet region (region III) the pressure is near the atmospheric value and, hence, liquid particles in the jet move inertially. The flow inside the region was analysed by Howison et al. (1991) within the Wagner theory. It was shown that the jet motion is approximately one-dimensional and depends on that in the jet root. The influence of the jet motion on the flow inside the jet root may be neglected.

Here, the flows in regions I and II are analysed, and matched to each other and to the state of rest in region IV. Deflection of the shell is taken into account during the analysis of the liquid flow.

### 3. Elastic-shell vibrations

The elastic-shell vibrations satisfy the equations and boundary conditions

$$\ddot{w} + \alpha(w - v_\theta) + \beta(v_{\theta\theta\theta} + w_{\theta\theta\theta}) = \gamma p_0(\theta, t) \quad (-\pi < \theta < \pi), \tag{1}$$

$$\ddot{v} + \alpha(w_\theta - v_{\theta\theta}) - \beta(v_{\theta\theta} + w_{\theta\theta\theta}) = 0 \quad (-\pi < \theta < \pi), \tag{2}$$

$$v(\theta, 0) = w(\theta, 0) = 0 \quad (-\pi < \theta < \pi), \tag{3}$$

$$v_t(\theta, 0) = -\sin \theta, \quad w_t(\theta, 0) = -\cos \theta \quad (-\pi < \theta < \pi), \tag{4}$$

where

$$\alpha = \frac{E}{\rho_0 R^2 V^2 (1 - \nu^2)}, \quad \beta = \frac{E h_0^2}{12 \rho_0 R^4 V^2 h'^2 (1 - \nu^2)}, \quad \gamma = \frac{\rho h'}{\rho_0 h_0}, \quad R = \frac{R'}{h'}$$

see, e.g., Grigoliuk and Gorshkov (1974) or Ionina and Korobkin (1999). Here, an overdot denotes a derivative with respect to time,  $w$  and  $v$  stand for the radial and angular components of the absolute displacements of the shell elements, respectively,  $r$  and  $\theta$  are polar coordinates,  $\theta = 0$  corresponds to the lowest point of the body,  $h_0$  is the thickness of the shell,  $\rho_0$  is the density of the shell material,  $E$  is the elasticity modulus,  $\nu$  is Poisson's ratio,  $p(x, y, t)$  is the hydrodynamic

pressure, and  $p_0(\theta, t)$  is the external (hydrodynamic) load acting on the elastic shell. Within the contact region,  $|x| < c(t)$  and  $|\theta| < \theta_c(t)$ , one has  $p_0(\theta, t) = p(x(\theta, t), y(\theta, t), t)$ , where  $x(\theta, t)$  and  $y(\theta, t)$  are the horizontal and vertical coordinates of the point on the elastic cylinder,  $x(\pm\theta_c(t), t) = \pm c(t)$ . During the initial stage of the impact, the approximate formulae  $x \approx R\theta$ ,  $\theta_c(t) \approx c(t)/R$  may be used. The initial conditions, Eqs. (3) and (4) assume that the shell is undeformed before the impact and moves vertically.

Eqs. (1)–(4) correspond to the structural part of the problem. The coupled structural and hydrodynamic problem requires that the size of the contact region and the hydrodynamic pressure distribution along the wetted region be determined simultaneously.

**4. Liquid flow in the region I, beneath the shell**

Estimates of the liquid flow parameters and physical considerations indicate that, within region I ( $|x| < c(t)$ ,  $-1 < y < f(x, t)$ , where  $f(x, t)$  is the shape of the entering body), the pressure  $p$  and the horizontal component  $u$  of the velocity are approximately independent of  $y$  [see Korobkin (1995, pp. 47–50) for details].

The nondimensional equations for the liquid velocity  $\vec{u} = (u_1, u_2)$  of the liquid motion are

$$\frac{\partial u_1}{\partial t} + u_1 \frac{\partial u_1}{\partial x} = -\frac{\partial p}{\partial x}, \tag{5}$$

$$\frac{\partial u_1}{\partial x} + \frac{\partial u_2}{\partial y} = 0 \quad (|x| < c(t), \quad -1 < y < f(x, t)), \tag{6}$$

$$u_2 = f_x(x, t)u_1 + f_t(x, t) \quad (y = f(x, t), \quad |x| < c(t)), \tag{7}$$

$$u_2 = 0 \quad (y = -1, \quad |x| < c(t)). \tag{8}$$

Here,  $u_1 = u_1(x, t)$ ,  $p = p(x, t)$ ,  $u_2 = u_2(x, y, t)$ . Integration of system (6)–(8) yields

$$u_1(x, t) = \frac{-\int_0^x f_t(\xi, t) d\xi}{f(x, t) + 1}, \tag{9}$$

for the symmetrical case. The symbol  $u$  for horizontal component of the liquid velocity will be used below instead of  $u_1$ .

The pressure distribution over the contact line can be determined by integrating Eq. (5) and using Eq. (9) and the boundary condition  $p(c(t), t) = p_c(t)$ , where  $p_c$  is not known in advance. Integration yields

$$p(x, t) = p_c(t) + \frac{1}{2}[u^2(c, t) - u^2(x, t)] + \int_x^c u_t(\xi, t) d\xi. \tag{10}$$

The functions  $f(x, t)$  and  $c(t)$ , which define the shape of the body and the size of the contact region, are unknown in Eqs. (9) and (10).

**5. Liquid flow in region II and matching conditions**

The liquid flow in region II is analysed as in Korobkin (1995). Within this approach, the velocity of the body is neglected and the body surface is taken as a horizontal plate; see Fig. 3. The flow is assumed to be approximately

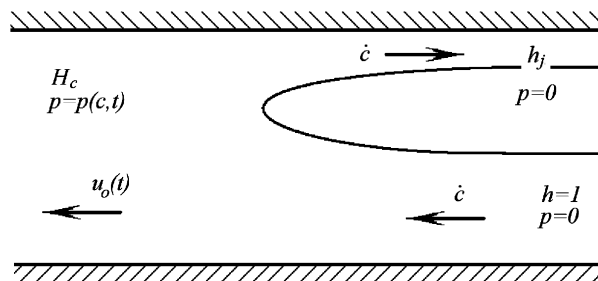


Fig. 3. Definition sketch for the flow in the jet root region.

quasi-stationary. The jet of thickness  $l$  moves to the left with velocity  $dc/dt$ . A part of the jet mass continues to move left between the two rigid horizontal plates, separated by the distance  $H_c = f(c, t) + 1$ . At left-hand side infinity, the pressure is  $p_c(t)$  and the horizontal velocity is  $u_0 = dc/dt - u(c, t)$ . Another part of the jet is deflected and forms a spray jet of thickness  $h_j$ . The dynamic condition at the free surface requires that the magnitude of the flow velocity at the free surface be constant. The jet horizontal velocity at infinity is then  $dc/dt$ ; see Tuck and Dixon (1989). Here, matching of the flow parameters in regions I and II was used. A detailed analysis of the flow can be obtained from conservation laws:

mass-conservation law:

$$\dot{c} = h_j \dot{c} + H_c u_0; \tag{11}$$

Bernoulli's equation (energy-conservation law):

$$(\dot{c})^2 = 2p_c + u_0^2; \tag{12}$$

momentum-conservation law:

$$(p_c + u_0^2)H_c = (\dot{c})^2(1 + h_j). \tag{13}$$

The three Eqs. (11)–(13) determine the three unknown functions  $h_j(t)$ ,  $\dot{c}(t)$ ,  $p_c(t)$ , as follows:

$$h_j(t) = (\sqrt{H_c} - 1)^2, \tag{14}$$

$$\dot{c}(t) = \frac{-\int_0^c f_t(\xi, t) d\xi}{2(H_c - \sqrt{H_c})}, \quad p_c(t) = \frac{(\int_0^c f_t(\xi, t) d\xi)^2}{2H_c^2(\sqrt{H_c} - 1)}. \tag{15}$$

It should be emphasized that the exact liquid flow in region II is not considered. The conservation laws in this region are only used to match the flow in the region beneath the body and the state of rest in the outer region, and to determine the turnover point  $c$ . The region  $(-c, c)$  is then considered as the effective contact region. Thus, Eqs. (14) and (15) define the flow in region I, the size of the contact region, and the pressure distribution along the contact line by virtue of Eqs. (9) and (10).

### 6. Normal mode method

The coupled hydroelasticity problem is solved here using the normal mode method. This approach is very convenient for description of elastic deformations of the body and was used before in numerous studies, e.g., Ionina and Korobkin (1999), Korobkin and Khabakhpasheva (2006) or Korobkin et al. (2008). If a structure is complex or its displacement and large, finite element method can be more appropriate for the modelling of the structure dynamics, see e.g., Korobkin et al. (2006) or Lu et al. (2000).

Within the normal mode method, the solution of the boundary-value problem, Eqs. (1)–(4), is sought in the form

$$p(\theta, 0, t) = \frac{p_0}{2} + \sum_{n=1}^{\infty} p_n(t) \cos n\theta, \\ w(\theta, t) = \frac{a_0}{2} + \sum_{n=1}^{\infty} a_n(t) \cos n\theta, \quad v(\theta, t) = \sum_{n=1}^{\infty} b_n(t) \sin n\theta, \tag{16}$$

where  $-\pi < \theta < \pi$ , and the principal coordinates  $a_n(t)$  and  $b_n(t)$  define the elastic deformation of the shell. During the initial stage of the impact, the approximate formula  $\theta = x/R$  may be used. The shape of the shell is given by

$$f(x, t) = R - \sqrt{R^2 - x^2} + \frac{a_0}{2} + \sum_{n=1}^{\infty} a_n(t) \cos \frac{nx}{R}. \tag{17}$$

Eq. (9) yields

$$u(x, t) = \frac{U(x, \ddot{a}(t))}{H(x, \ddot{a}(t))}, \tag{18}$$

where

$$U(x, \ddot{a}(t)) = -\frac{\dot{a}_0 x}{2} - R \sum_{n=1}^{\infty} \frac{\dot{a}_n(t)}{n} \sin \frac{nx}{R}, \quad H(x, \ddot{a}(t)) = f(x, t) + 1.$$

Eqs. (14) and (15) then take the form

$$\dot{c} = \frac{U(c, \dot{\bar{a}}(t))}{2(H_c - \sqrt{H_c})}, \quad p_c(t) = \frac{U^2(c, \dot{\bar{a}}(t))}{2H_c^2(\sqrt{H_c} - 1)}, \quad H_c = H(c, \bar{a}(t)).$$

The coefficients  $p_m(t)$  of the first expansion in Eq. (16) can be determined via multiplication of Eq. (10) by  $\cos(nx/R)$  and integration with respect to  $x$  within the range  $-c \leq x \leq c$ . After integration,  $p_m(t)$  is obtained in the form

$$p_m(t) = K_m(t, c(t), \bar{a}(t), \dot{\bar{a}}(t)) - \sum_{n=0}^{\infty} S_{nm}(t, c(t), \bar{a}(t)) \dot{a}_n(t), \tag{19}$$

where

$$K_n(t, c(t), \bar{a}(t), \dot{\bar{a}}(t)) = \frac{2}{\pi R} \int_0^c K(t, c(t), x, \bar{a}(t), \dot{\bar{a}}(t)) \cos \frac{nx}{R} dx, \quad n = 0, 1, 2, \dots, \tag{20}$$

$$K(t, c(t), x, \bar{a}(t), \dot{\bar{a}}(t)) = \frac{(U(c, \dot{\bar{a}}))^2}{2H_c^2(\sqrt{H_c} - 1)} + \frac{1}{2} \left[ \frac{(U(c, \dot{\bar{a}}))^2}{(H(c, t, \bar{a}))^2} - \frac{(U(x, \dot{\bar{a}}))^2}{(H(x, t, \bar{a}))^2} \right] - \int_x^c \frac{U(\xi, \dot{\bar{a}}) \left[ \frac{\dot{a}_0}{2} + \sum_{n=1}^{\infty} \dot{a}_n \cos \frac{n\xi}{R} \right] d\xi}{(H(\xi, \bar{a}))^2}, \tag{21}$$

$$S_{00}(t, c(t), \bar{a}(t)) = \frac{2}{\pi R} \int_0^c \frac{\xi^2}{H(\xi, \bar{a})} d\xi,$$

$$S_{0m}(t, c(t), \bar{a}(t)) = S_{m0}(t, c(t), \bar{a}(t)) = \frac{2}{\pi m} \int_0^c \frac{\xi \sin \frac{m\xi}{R}}{H(\xi, \bar{a})} d\xi,$$

$$S_{nm}(t, c(t), \bar{a}(t)) = \frac{2R}{\pi nm} \int_0^c \frac{\sin \frac{n\xi}{R} \sin \frac{m\xi}{R}}{H(\xi, \bar{a})} d\xi, \quad n, m = 1, 2, 3, \dots \tag{22}$$

The system of equations (1) and (2) can be expanded to obtain expressions for the principal coordinates  $a_n(t)$  and  $b_n(t)$ ,  $n = 0, 1, 2, \dots$

$$\ddot{a}_n + a_n(\alpha + \beta n^4) - b_n(\alpha n + \beta n^3) - \gamma p_n = 0, \tag{23}$$

$$\ddot{b}_n - a_n(\alpha n + \beta n^3) + b_n(\beta n^2 + \alpha n^2) = 0, \tag{24}$$

Eq. (19) can be used and combined with the second derivatives  $\ddot{a}_n(t)$ . Following [Ionina and Korobkin \(1999\)](#), an infinite system of ordinary differential equations is obtained for the principal coordinates  $\bar{a} = (a_0, a_1, a_2, \dots)^T$ ,  $\bar{b} = (b_0, b_1, b_2, \dots)^T$  and auxiliary vector-functions  $\bar{q} = (q_0, q_1, q_2, \dots)^T$ ,  $\bar{r} = (r_0, r_1, r_2, \dots)^T$ :

$$\dot{\bar{q}} = (I + \gamma S)^{-1} (\gamma \bar{K}(t, c(t), x, \bar{a}(t), \dot{\bar{a}}(t)) - D_1 \bar{a} + D_2 \bar{b}), \tag{25}$$

$$\dot{\bar{r}} = D_2 \bar{a} - D_3 \bar{b}, \tag{26}$$

$$\dot{\bar{a}} = \bar{q}, \quad \dot{\bar{b}} = \bar{r}, \tag{27,28}$$

where

$$\bar{K} = (K_0, K_1, K_2, \dots), \quad D_1 = \text{diag}(\alpha + \beta n^4), \quad D_2 = \text{diag}(\alpha n + \beta n^3), \quad D_3 = \text{diag}(\alpha n^2 + \beta n^2).$$

Initial conditions at  $t = 0$  are

$$c = 0, \tag{29}$$

$$q_n = 0, \quad r_n = 0, \quad a_n = 0, \quad b_n = 0, \quad n \neq 1, \tag{30}$$

$$q_n = -1, \quad r_n = -1, \quad a_n = 0, \quad b_n = 0, \quad n = 1. \tag{31}$$

The system of equations (25)–(31) is solved numerically using the fourth-order Runge–Kutta method with uniform step  $\Delta t$ . The integrals in Eqs. (20)–(22) are evaluated numerically using the parabolic approximation.

## 7. Numerical results and discussion

The following shell characteristics are considered:

- (i) radial deflection of the shell  $w(\theta, t)$ , Eq. (16);
- (ii) full deflection of the shell, including both normal and radial deflections

$$W(x, t) = w \cos \theta + v \sin \theta;$$

- (iii) full form of the shell, including both normal and radial deflections

$$f(x, t) = R - \sqrt{R^2 - x^2} + W(\theta(x));$$

- (iv) circle bending moment

$$M = -\frac{Eh_0^3}{12(1-\nu^2)}\kappa,$$

which is proportional to the curvature

$$\kappa = -\frac{1}{R^2} \left( \frac{\partial v}{\partial \theta} + \frac{\partial^2 w}{\partial \theta^2} \right);$$

- (v) strains at the outer fibre

$$\varepsilon = \frac{12M}{Eh_0};$$

- (vi) specific circle normal force

$$N = -\frac{Eh_0}{1-\nu^2}\varepsilon_{cl},$$

which is proportional to the strain at a central line in the normal direction

$$\varepsilon_{cl} = \frac{1}{R} \left( \frac{\partial v}{\partial \theta} - w \right).$$

A first series of numerical simulations are performed for the conditions of the experiment reported by [Shibue et al. \(1994\)](#) in their investigation of the impact of a cylindrical shell in deep water. These experimental conditions are also considered by [Ionina and Korobkin \(1999\)](#). A cylindrical shell with outer radius  $R = 0.156$  m and thickness  $h_0 = 5.1$  mm is considered. The shell, made of steel with  $E = 206 \times 10^9$  Pa,  $\nu = 0.3$ ,  $\rho_0 = 8067$  kg/m<sup>3</sup>, falls with initial impact velocity  $V = 3.5$  m/s, onto a layer of water (density  $\rho = 1000$  kg/m<sup>3</sup>). Results of calculations, obtained using 15 modes, are reported for several values of the thickness of the water layer between  $h' = 10$  and 100 mm. A nondimensional time step  $\Delta t = 5 \times 10^{-4}$ , which corresponds to  $(h'/100 \text{ mm}) \times 1.5 \times 10^{-4}$  s in dimensional variables, is chosen. The time unit is a millisecond for every figure.

[Fig. 4](#) shows the evolution of the strain (in microstrains) at the lower point ( $\theta = 0$ ) for  $h' = 100$  mm. The results shown in [Fig. 4](#) are in general agreement with both the results obtained in [Ionina and Korobkin \(1999\)](#) and the experimental results reported in [Shibue et al. \(1994\)](#). It should be noticed that the present results are obtained within the framework of a shallow water model, whereas the results of [Ionina and Korobkin \(1999\)](#) correspond to a deep water model and the experimental results reported by [Shibue et al. \(1994\)](#) are obtained for a finite water layer. Better agreement among these distinct results can hardly be expected. Furthermore, the shallow water model accurately predicts the maximum strain, and the instant of time for which the maximum strain is achieved, even if the use of the shallow water model may be questioned for the ratio between the shell radius and the thickness of the water layer considered here. Good agreement was also found for the maximum strain and related instants of time at the points that correspond to the angles  $10^\circ$ ,  $20^\circ$  and  $30^\circ$ .

These results allow us to conclude that only a thin layer of the water is caused to flow at the initial stage of the impact of a flat body. The liquid flow below some value of the depth continues to be at rest.

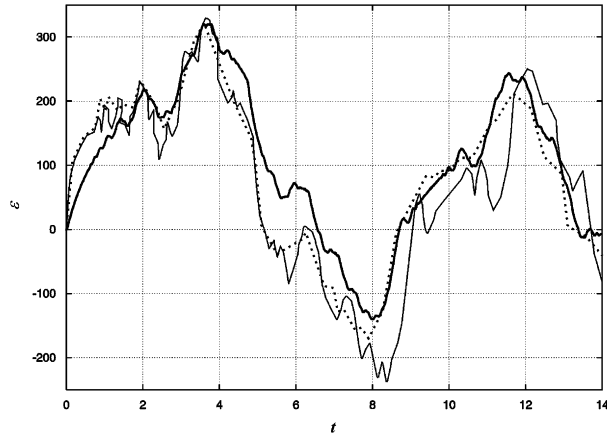


Fig. 4. Comparison of the evolutions of the strain at the point  $\theta = 0$  predicted by the present study for finite water depth (solid thick line) and for deep water by Ionina and Korobkin (1999) (thin line), and observed experimentally by Shibue et al. (1994) (dotted line).

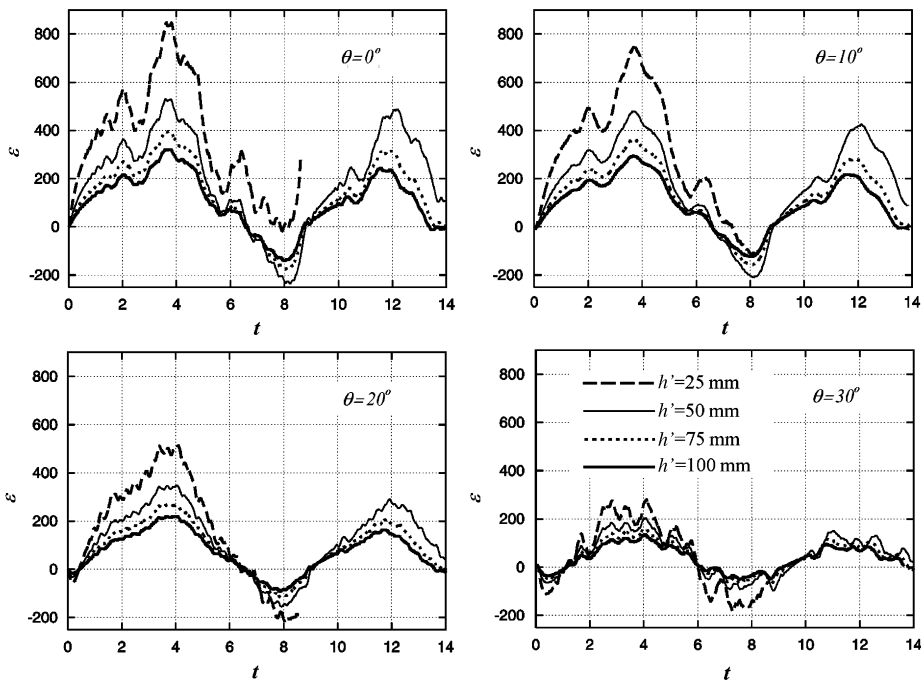


Fig. 5. Evolution of the strain at the points  $\theta = 0^\circ, 10^\circ, 20^\circ$  and  $30^\circ$  for water depths  $h' = 25, 50, 75$  and  $100$  mm.

It should be noticed that Korobkin's approach is based on two main geometrical assumptions:

- The liquid flow beneath the body is described by the shallow water model, in which only the horizontal component of the liquid velocity is taken into account.
- In the turnover region (region II), the body surface is assumed to be flat.

Neither of these assumptions is valid near the edges of the contact region for a shell of radius 150 mm that penetrates a liquid layer at a depth greater than 10 mm (for which one has  $c' \geq 70$  mm and  $\theta \geq 30^\circ$ ). For the considered case of the

steel shell impact, these conditions yield  $t' \geq 4$  ms. Nevertheless, agreement for the evolution of strain can be observed in Fig. 4. This agreement provides an indirect confirmation of the usefulness of the present approach, even for values of parameters for which the validity of the model may be questioned.

Fig. 5 shows the evolution of the strains obtained for water layer thicknesses equal to  $h' = 25, 50, 75$  and  $100$  mm and for several points of the shell that correspond to angles  $\theta = 0^\circ, 10^\circ, 20^\circ$  and  $30^\circ$ . The time histories for the four thicknesses of the water layer and the four points considered here are similar in that local maximums and minimums occur at the same instants of time. However, the absolute values of the maximal strain are different, and are larger for thinner layers of water.

In this high-rigidity case, full deflection of the shell corresponds to straight-line motion of the shell, without visible change of the shell form. The strain along a central line in the normal direction was found to be negligible (less than  $0.06$  microstrain) during the impact.

Fig. 6, 8 and 9 show results of calculations, for an impact velocity  $V = 3.5$  m/s and a water layer thickness  $h' = 25$  mm, for different values of the thickness of the cylindrical steel shell, which varies between  $h_0 = 1.25$  and  $5.1$  mm. Calculations are performed using 15 modes and a nondimensional time step taken as  $\Delta t = 5 \times 10^{-4}$ , which corresponds to  $0.75 \times 10^{-5}$  s.

Fig. 6(a) shows the evolution of the immersion depth of the lowest point ( $\theta = 0^\circ$ ) for several values of the shell thickness. The thin straight line indicates the immersion that corresponds to impact velocity  $V = 3.5$  m/s without water. The velocity of immersion can be seen to be smaller for thinner shells. Fig. 6(b) shows the form of the shell at the lowest

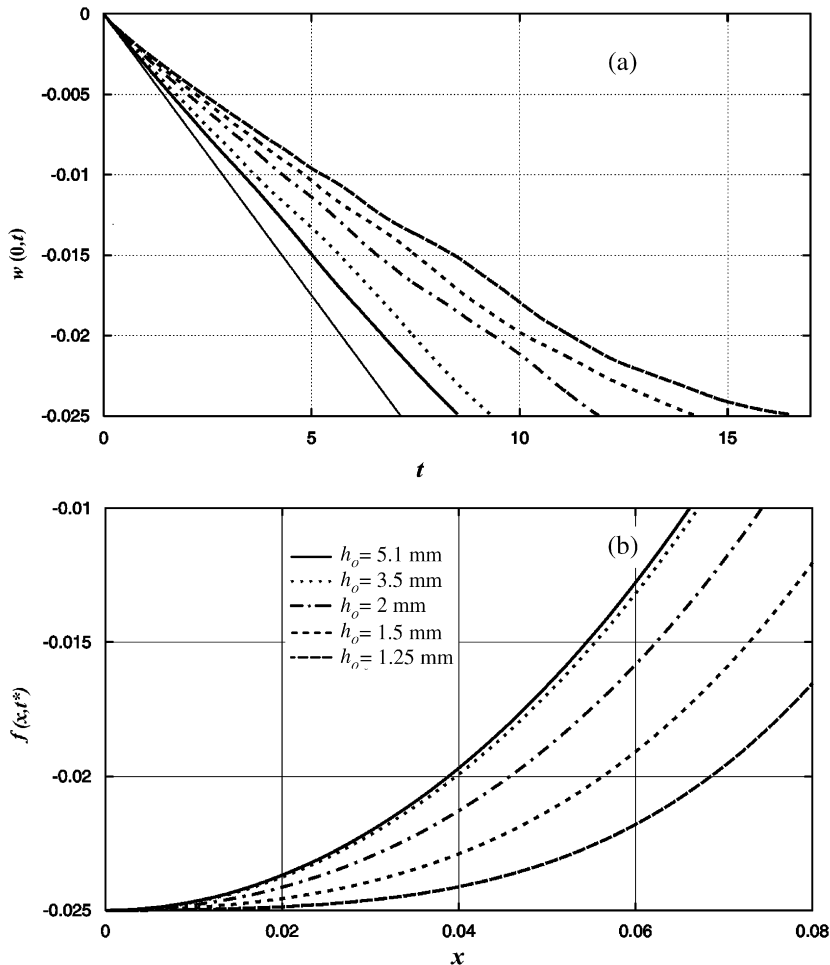


Fig. 6. Position of the point of the shell  $\theta = 0^\circ$  as a function of time (a) and shape of the shell at the instant of time  $t^*$  when the shell reaches the bottom (b) for different values of the shell thickness.

point, when the shell reaches the bottom of the layer of water. The line for  $h_0 = 5.1$  mm is very close to a circle. However, thinner shells are more flat. It should be noted that the instants of time  $t^*$  at which the shell reaches the bottom are different for the different cases considered in this figure.

A shell with thickness smaller than 1.25 mm does not reach the bottom of the water layer. As the shell enters the water, the shape of the lower portion of the shell flattens, the velocity of immersion is reduced, and at some instant of time the size of the wetted region is also reduced (see Fig. 7). Within the present theory, the matching conditions for the flow subregion II imply that the velocity of wetting must be positive. Calculations cannot be pursued if the size of the contact region begins to decrease—a behaviour that corresponds to exit or “reflection” of the shell from the water layer, before the shell reaches the bottom. Similar results were obtained for an aluminium shell with  $E = 71 \times 10^9$  Pa,  $\rho_0 = 2700$  kg/m<sup>3</sup>, outer radius  $R = 0.156$  m, a shell thickness smaller than 2.5 mm and a water depth smaller than 25 mm.

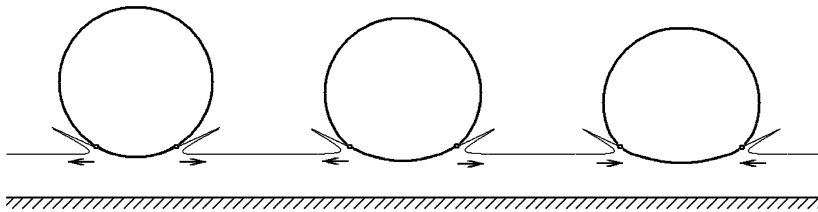


Fig. 7. Sketch illustrating the reflection for the case of the steel shell.

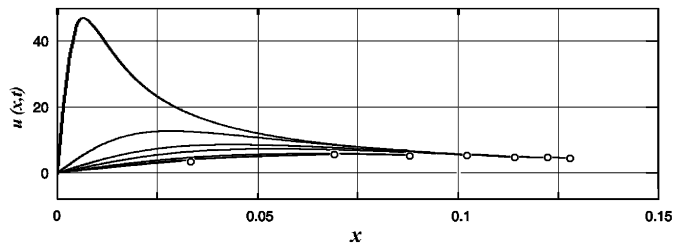


Fig. 8. Distribution of the horizontal component of the liquid velocity beneath the shell at selected time instants. The extent of the wetted region for every time instant is indicated by circles.

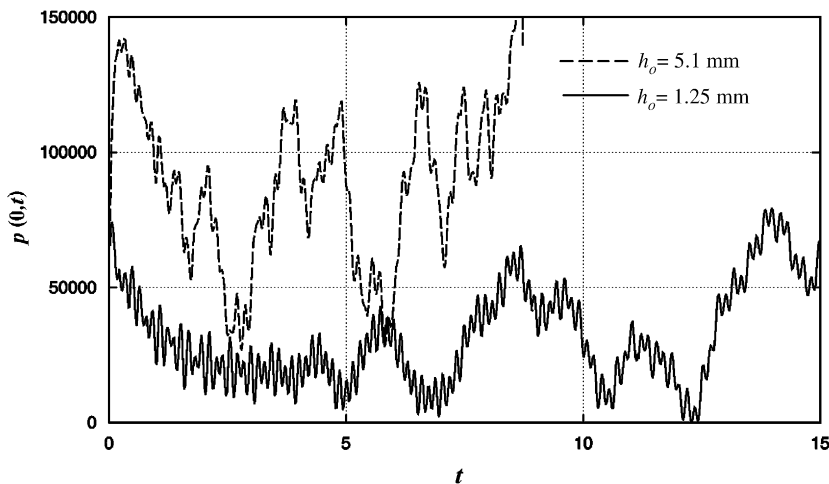


Fig. 9. Time history of the pressure at the point  $\theta = 0^\circ$  for a shell thickness: —,  $h_0 = 1.25$  mm; - - -,  $h_0 = 5.1$  mm.

The evolution of the horizontal component of the liquid velocity beneath the shell is depicted in Fig. 8 for several instants of time. Each time is associated with a particular contact region,  $x = c'$ , as indicated by a cycle. The lines correspond to times in the range  $0.018 \text{ ms} < t' < 8.65 \text{ ms}$ , selected to show the evolution of the velocity as clearly as possible. The horizontal fluid velocity increases sharply as the thickness of the liquid layer becomes smaller. This figure corresponds to a shell thickness  $h_0 = 5.1 \text{ mm}$ . Calculations for other values of the steel shell thickness yield a similar variation of the liquid velocity with respect to time.

Fig. 9 depicts the time history of the pressure at the lowest point of the shell ( $\theta = 0^\circ$ ). The solid and dashed lines correspond to a shell thickness  $h_0 = 1.25$  and  $5.1 \text{ mm}$ , respectively. The pressure varies very rapidly with time, although the pressure distribution along the wetted region is smooth at every instant of time. The pressure is higher for thicker shells. It is interesting that the pressure at the first instant of time  $p(0, 0)$  is similar in both cases and approximately equal to  $7 \times 10^4 \text{ Pa}$ . This pressure is about half the pressure for a rigid body, which is given by the expression  $p(x, t) \approx 3\rho V^2 R'/h'$ ; see Korobkin (1995).

Another series of numerical simulations are performed for an elastic shell made of glass fibre plastic with  $E = 3 \times 10^9 \text{ Pa}$ ,  $\nu = 0.3$  and  $\rho_0 = 1180 \text{ kg/m}^3$ . The outer radius of the cylinder is  $R = 0.156 \text{ m}$  and the thickness of the cylinder is  $h_0 = 1 \text{ mm}$ . Due to the high flexibility of this shell, it is necessary to use a greater number of modes than for the steel shell. Thirty modes are used for the present calculations. The nondimensional time step is taken as  $\Delta t = 10^{-4}$ .

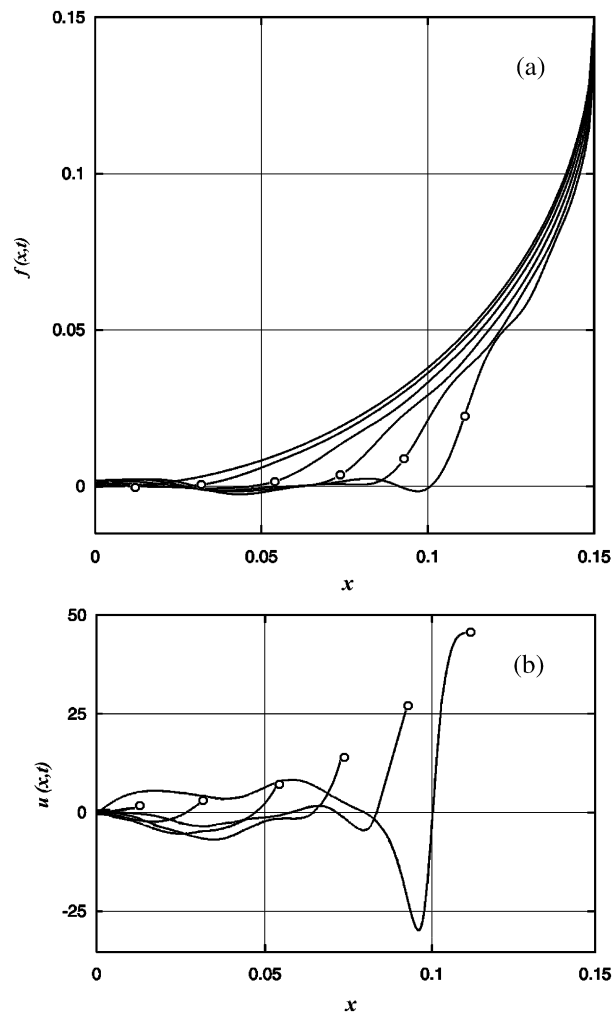


Fig. 10. (a) Evolution of the form of the shell and (b) of the horizontal component of the liquid velocity for the glass fibre plastic shell at selected time instants.  $V = 3.5 \text{ m/s}$ ,  $h' = 10 \text{ mm}$ .

The results depicted in Fig. 10 correspond to the thickness of the water layer  $h' = 10$  mm and the impact velocity  $V = 3.5$  m/s. Fig. 10(a) shows the evolution of the shell form, and Fig. 10(b) shows the horizontal component of the liquid velocity beneath the shell. The circles indicate the variation of the size of the contact region  $c'$  with respect to time, as in Fig. 8. It can be seen that the shell does not enter the water and that the shell form flattens at the contact of water, which remains flat. The horizontal velocity of the water is quite high because the thickness of the water layer is small. It is interesting that the liquid velocity is negative, which means that the liquid moves toward the axis of symmetry of the shell, for some wetted regions and some instants of time. It should be noticed that the curves with  $c' \approx 0.09$  and  $0.115$  m in the figure actually do not satisfy the second geometrical assumption. These numerical results indicate the behaviour of the liquid flow and shape of the shell during the end of the impact process only.

Figs. 11–13 correspond to “soft” impact conditions; specifically, the thickness of the water layer is  $h' = 10$  mm and the impact velocity is  $V = 1.5$  m/s. The shell thickness is  $h_0 = 2$  mm. A dimensionless time step  $\Delta t = 10^{-5}$  was used. Calculations were performed using both 35 modes and 50 modes to confirm convergence of the procedure. Fig. 11(a) shows the evolution of the shell form, and Fig. 11(b) depicts the horizontal component of the liquid velocity beneath the shell, again plotted as in Fig. 8. In this case, the shell is finally submerged in the water layer and reaches the bottom of the water layer. The shell does not touch the bottom at the central point of the contact region ( $\theta = 0^\circ$ ), but at a point

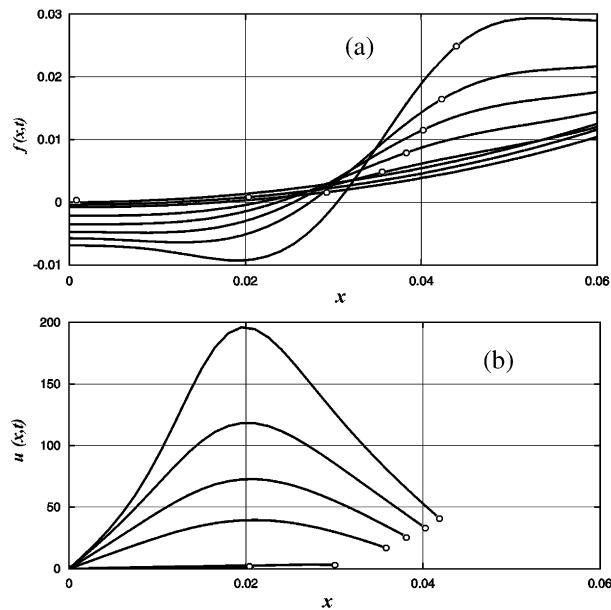


Fig. 11. (a) Evolution of the form of the shell and (b) of the horizontal component of the liquid velocity for the glass fibre plastic shell at selected time instants.  $V = 1$  m/s,  $h' = 25$  mm.

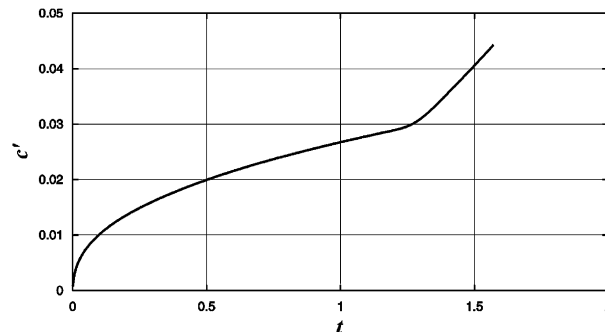


Fig. 12. Evolution of the size of the contact region as a function of time.

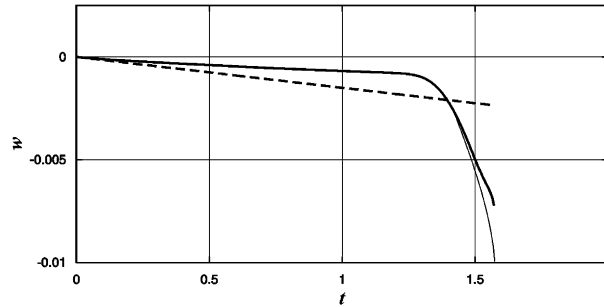


Fig. 13. Evolution of the position of the central point  $\theta = 0^\circ$  as a function of time (thick solid line) and lowest point of the shell (thin line).

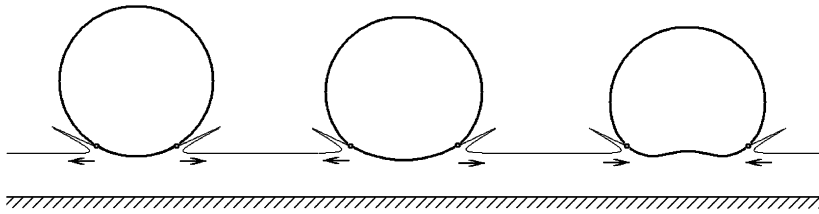


Fig. 14. Sketch for the illustration of the “reflection” for the case of the glass fibre plastic shell.

with  $\theta^* \approx 0.16^\circ$ . The effect of “fluid capture” occurs in this case. This behaviour reflects the influence of high modes (modes with  $n = 18, 19, 20$ ) and therefore cannot be observed if only a small number of modes is used. The liquid velocity reaches its maximum value near the same point  $\theta^*$ .

Fig. 12 depicts the variation of the size  $c'$  of the contact region as a function of time. Initially,  $c'(t)$  varies in accordance with the parabolic law, but  $c'$  increases rapidly after some instant  $t^*$ . The position of the central point ( $\theta = 0^\circ$ ) as a function of time is indicated in Fig. 13 by a thick solid line. The dashed line in this figure corresponds to immersion with constant velocity  $V = 1.5$  m/s and the thin line indicates depth of maximal submergence of the shell. Initially, the shell penetrates the liquid layer with velocity equal to approximately half the impact velocity; however, the velocity of the center point and the maximum submergence velocity increase rapidly after the time instant  $t^*$ .

If the impact velocity is smaller than 0.75 m/s, a fairly complicated sequence of events takes place (see Fig. 14). At first, the shell enters the liquid layer very slowly and the shape of the lower part of the shell flattens. Subsequently, the shape of the shell changes rapidly, and the shell moves toward the bottom of the water layer at high velocity. Then the numerical calculations show that the shell does not reach the bottom, because the lowest point of the shell moves upward and local maxima of the shell form occur at the point  $\theta = 0$ . Finally, the size of the contact region decreases. This behaviour indicates that the shell moves upward, and is “reflected” before reaching the bottom.

## 8. Conclusion

The impact of a thin elastic cylindrical shell on a thin layer of water was studied as a coupled hydroelasticity problem in which the flow of water beneath the shell and the shell deformations are determined simultaneously. The elastic deformation of the shell was analysed using the normal modes method. The liquid flow was analysed using Korobkin’s approach, via the method of matched asymptotic expansions. This fluid–structure coupled analysis leads to a system of nonlinear differential equations for the evolution of principal coordinates of the shell shape and the fluid hydrodynamic pressure. The solution of this evolution system provides both the deformation and stresses for the shell, the size of the contact region between the shell and the liquid, and the liquid flow.

A main result of the analysis is that shallow-water impact is more dangerous than deep-water impact because stresses and the deformation of the shell increase as the thickness of the water layer decreases. But starting from some

relatively large depth of the water, maximal values of the stresses and deflections remain constant with increasing water depth.

In the case of a glass-fibre plastic shell, three distinct regimes were found. For a high impact velocity and a thin layer of water, the lower part of the shell flattens and the shell does not enter the water. For a moderate impact velocity, the lower part of the shell initially flattens. This initial stage is followed by high vibratory motions of the shell, which moves rapidly downward. The shell may touch the bottom of the layer of water at a point located off the centerline, rather than at the central point. For a low impact velocity and relatively deep water, the rapid downward motion of the shell is followed by a rapid increase of the size of the shell-liquid contact region and upward motion of the shell's central point. These regimes cannot be found if only the first few modes of the vibratory motions of the shell are considered.

These regimes were not found for a (relatively rigid) steel shell. For a thin steel shell and a thin layer of water, the size of the shell-water contact region was found to decrease, which indicates that the shell moves upward before reaching bottom.

### Acknowledgments

The author is most grateful to Alexander Korobkin for suggesting the problem and for many useful discussions. The work was supported by grants from the Russian Fund of Basic Research (07-08-00145) and the Foundation "Leading Scientific Schools" (NSh-2260.2008.1).

### References

- Arai, M., Miyachi, T., 1998. Numerical study of the impact of water on cylindrical shells, considering fluid–structure interactions. In: Proceedings of Conference on Practical Design of Ships and Mobile Structure (PRADS'98), The Hague, Netherlands, pp. 59–68.
- Faltinsen, O.M., Landrini, M., Greco, M., 2004. Slamming in marine applications. *Journal of Engineering Mathematics* 48, 187–217.
- Greenhow, M., 1988. Water-entry and -exit of a horizontal circular cylinder. *Applied Ocean Research* 10, 191–198.
- Grigoliuk, E.I., Gorshkov, A.G., 1974. Non-stationary hydroelasticity of the shell. "Shipbuilding," Leningrad, USSR (in Russian).
- Howison, S.D., Ockendon, J.R., Wilson, S.K., 1991. Incompressible water-entry problems at small deadrise angles. *Journal of Fluid Mechanics* 222, 215–230.
- Howison, S.D., Ockendon, J.R., Oliver, J.M., 2002. Deep- and shallow-water slamming at small and zero deadrise angles. *Journal of Engineering Mathematics* 42, 373–388.
- Ionina, M.F., Korobkin, A.A., 1999. Water impact on cylindrical shell. In: Proceedings of 14th International Workshop on Water Waves and Floating Bodies, Michigan, USA, pp. 44–47.
- Khabakhpasheva, T.I., Korobkin, A.A., 1997. Wave impact on elastic plates. In: Proceedings of 12th International Workshop on Water Waves and Floating Bodies, Carry-le-Rouet, France, pp. 135–138.
- Korobkin, A.A., 1995. Impact of two bodies one of which is covered by a thin layer of liquid. *Journal of Fluid Mechanics* 300, 43–58.
- Korobkin, A.A., Khabakhpasheva, T.I., 2006. Regular wave impact onto an elastic plate. *Journal of Engineering Mathematics* 55, 127–150.
- Korobkin, A.A., Gueret, R., Malenica, S., 2006. Hydroelastic coupling of beam finite element model with Wagner theory of water impact. *Journal Fluids and Structures* 22, 493–504.
- Korobkin, A.A., Khabakhpasheva, T.I., Wu, G.X., 2008. Coupled hydrodynamic and structural analysis of compressible jet impact onto elastic panels. *Journal Fluids and Structures* 24 (7), 1021–1041.
- Lu, C.H., He, Y.S., Wu, G.X., 2000. Coupled problem of nonlinear interaction between fluid and structure during impact. *Journal Fluids and Structures* 14, 127–146.
- Shibue, T., Ito, A., Nakayama, E., 1994. Structural response analysis of cylinders under water impact. In: Proceedings of International Conference on Hydroelasticity in Marine Technology, Trondheim, Norway, pp. 221–228.
- Sun, H., Faltinsen, O.M., 2006. The fluid–structure interaction during the water impact of a cylindrical shell. In: Proceedings of 4th International Conference on Hydroelasticity in Marine Technology, Wuxi, China, pp. 149–158.
- Tuck, E.O., Dixon, A., 1989. Surf-skimmer planing hydrodynamics. *Journal of Fluid Mechanics* 205, 581–592.
- Von Kármán, T., 1929. The impact of seaplane floats during landing. NACA, Technical Note 321, Washington, DC, USA, pp. 309–313.
- Wagner, H., 1932. Über Stoss- und Gleitvorgänge an der Oberfläche von Flüssigkeiten. *Zeitschrift für Angewandte Mathematik und Mechanik* 12, 193–215.
- Zhu, X., Faltinsen, O.M., Hu, C., 2005. Water entry and exit of a horizontal circular cylinder. In: Proceedings of 24th International Conference on Offshore Mechanics and Arctic Engineering (OMAE), Halkidiki, Greece, CD-Rom.